Published in final edited form as:
Arthritis Rheum. 2012 June ; 64(6): 1899–1908. doi:10.1002/art.34370.

Quantitative Imaging of Cartilage and Bone Morphology, Reactive Oxygen Species, and Vascularization in a Rodent Model of Osteoarthritis

Liqin Xie, Ph.D.[+], **Angela S.P. Lin, M.S.**[+], **Kousik Kundu, Ph.D.**[#], **Marc E. Levenston, Ph.D.**[*], **Niren Murthy, Ph.D.**[#], and **Robert E. Guldberg, Ph.D.**[+,1]

[+]George W. Woodruff School of Mechanical Engineering, 315 Ferst Drive, Georgia Institute of Technology, Atlanta, GA 30332-0405

[#]Wallace H. Coulter Department of Biomedical Engineering, 313 Ferst Drive, Georgia Institute of Technology, Atlanta, GA 30332-0535

[*]Department of Mechanical Engineering, 233 Durand Building, Stanford University, Stanford, CA 94305-4038

Abstract

Objective—To assess temporal changes in cartilage and bone morphology, reactive oxygen species (ROS), and vascularization in mono-iodoacetate (MIA)-induced osteoarthritis (OA) in rats via advanced imaging methodologies.

Methods—Right knees of male 8-week old Wistar rats were injected with 1mg MIA in 50μl saline and left knee controls injected with 50μl saline. After 1, 2, and 3 weeks (n=5 each), changes in cartilage morphology and composition were quantified using equilibrium partitioning of an ionic contrast agent microcomputed tomography (EPIC-μCT) and changes in subchondral and trabecular bone were assessed by standard μCT. ROS were characterized via *in vivo* fluorescence imaging at 1, 11, and 21 days (n=5 each). At 3 weeks, after fluorescence imaging, alterations in knee joint vascularity were quantified with μCT after vascular contrast agent perfusion (n=5).

Result—Femoral cartilage volume, thickness, and proteoglycan content were significantly decreased in MIA injected knees compared to controls, accompanied by loss of trabecular bone and erosion of subchondral bone surface. ROS quantities were significantly increased 1 day after MIA injection and were gradually relieved by 21 days. Vascularity in the whole knee and distal femora was significantly increased at 3 weeks after MIA injection.

Conclusion—Contrast-enhanced μCT and fluorescence imaging were combined to characterize articular cartilage, subchondral bone, vascularization, and ROS, providing unprecedented 3-D joint imaging and quantification for multiple tissues during OA progression. These advanced imaging techniques have the potential to become standardized methods for comprehensive evaluation of articular joint degeneration and characterization of therapeutics.

Introduction

Osteoarthritis (OA) is a highly prevalent and debilitating condition that affects multiple functionally integrated tissues within articular joints, including cartilage, subchondral bone,

[1]**Correspondence to:** Robert E. Guldberg, Ph.D., Institute for Bioengineering and Bioscience, 315 Ferst Drive, Georgia Institute of Technology, Atlanta, GA 30332-0405, 404-894-6589 (P), 404-385-1397 (F), robert.guldberg@me.gatech.edu.

Conflict of Interest Statement
The authors have no conflicts of interest to disclose.

trabecular bone, synovium, and blood vessels (1). The pathophysiologic interactions among integrated joint tissues during initiation and progression of OA are currently poorly understood.

Subchondral bone and articular cartilage are intimately related, such that alteration in one can affect the structure and functional integrity of the other (2–4). Abnormalities in subchondral bone, such as changes of bone mineral density and bone turnover, have been suggested to contribute to the development of OA (2, 5–8). Subchondral bone serves as a passive shock absorber for the joint, blunting the effects of abnormally high mechanical loads that can damage the cartilage (9). When subchondral bone becomes thicker and sclerotic, its shock-absorbing capacity decreases (9). Although the exact causes of OA are not yet fully understood, a mechanical insult to the joint is regarded as a critical extrinsic risk factor to initiate OA (9). Recently, studies in animal models have provided longitudinal evaluations monitoring quantitative changes in cartilage and bone (10), which can help elucidate the etiopathogenesis of OA and to find effective therapies.

In contrast to inflammatory rheumatoid arthritis (RA), OA was formerly classified as a noninflammatory disease (11). This concept has been recently revised, and it is now understood that synovial inflammation, or synovitis, plays a critical role in the symptoms and progression of OA (12). Synovial inflammation, as evidenced by stiffness, pain, and effusion, is characterized by an infiltration of neutrophils, T lymphocytes, and monocytes (13), and can be assessed by MRI, ultrasound, arthroscopy, and biopsy (11). Synovial inflammation is further supported by the fact that non-steroidal anti-inflammatory drugs alleviate osteoarthritic symptoms and may be more effective than simple analgesics (11, 14). Synovitis can be induced by cartilage breakdown products, and may increase the likelihood of meniscal and subchondral bone changes (15).

Synovial inflammation is typically accompanied by angiogenesis, and both can be triggered by the same molecular events (16). Angiogenesis is demonstrated by the growth of new blood vessels from the subchondral bone to the articular cartilage during OA progression. Inflammatory cells such as macrophages can secrete and stimulate other cells (such as endothelial cells and fibroblasts) to secrete angiogenic factors such as vascular endothelial growth factor (VEGF)(12). Angiogenesis and synovial inflammation are closely associated in OA, and may contribute to the progression of cartilage degeneration and bone remodeling (17, 18) in part by redistributing blood vessels (19).

The responses of individual tissues in the knee joint have been studied in rat monosodium iodoacetate (MIA)-induced models of OA (20), but quantitative assessments of changes in articular cartilage, bone, vascularization, and reactive oxygen species (ROS) have not been performed together to determine correlations between the affected joint tissues. The objective of this study was to assess temporal changes in multiple integrated tissues of the knee joint as well as the interactions of these tissue changes during progression of OA in a MIA-induced rat OA model using advanced imaging methodologies. Changes in 3D cartilage morphology and composition were quantified using equilibrium partitioning of an ionic contrast agent micro-CT imaging (EPIC-μCT); changes in subchondral and trabecular bone were assessed by standard high resolution micro-CT analysis; ROS during OA progression were characterized via *in vivo* fluorescence imaging; and alterations in the vascularity of knee joint tissues were quantified using micro-CT after perfusion of a vascular contrast agent.

Methods

Assessment of Cartilage and Bone

The Georgia Institute of Technology Institutional Animal Care and Use Committee approved experimental procedures (IACUC protocol A06005). For fifteen male 8-week old Wistar rats (Charles River Laboratories, Sparks, NV), anesthesia was induced with 5% isoflurane inhalation and maintained at 2% isoflurane. 1mg of MIA (Sigma-Aldrich, St. Louis, MO) in 50μl saline was injected through the infrapatellar ligament of the right knee, with the left knee injected with 50μl saline as a control. Rats were euthanized via CO_2 inhalation at 1, 2, and 3 weeks after MIA injection (n=5 each). The femora were harvested, dissected free of surrounding tissues, and stored in phosphate buffered saline (PBS) solution with 1% proteinase inhibitors (PI, Cocktail I, CalBiochem, San Diego, CA) at 4°C (21).

The distal femora were pre-scanned for bone structure prior to incubation with contrast medium. For EPIC-μCT (as described in previous work), the distal femur was then immersed in 2ml of 40% Hexabrix 320 contrast agent (Covidien, Hazelwood, MO) and 60% PBS at 37 C for 30 minutes (21, 22) and gently patted dry before scanning. Samples were scanned using a μCT 40 (Scanco Medical, Brüttisellen, Switzerland) at 45 kVp, 177 μA, 200 ms integration time, and a voxel size of 16 μm.

Following scanning, femora were fixed in 10% neutral buffered formalin overnight and decalcified in 2.5% formic acid (pH 4.2) for 10 days. Dehydrated samples were embedded in glycol methacrylate according to the manual of the JB-4 embedding kit (Polysciences, Warrington, PA). For comparison with EPIC-μCT images, sagittal sections were cut at 8μm thickness and one section through the center of each condyle was examined. Sections were stained for sGAGs via sequential exposure to a 0.2% aqueous solution of Fast Green (1 min), 1% glacial acetic acid in 70% ethanol (10s), deionized water (1 min) and 0.5% safranin-O in distilled water (5 min).

In Vivo Quantification of Reactive Oxygen Species

Five male 8-week old Wistar rats were anaesthetized with isoflurane inhalation, and 1mg of MIA in 50μl saline was injected through the infrapatellar ligament of the right knee, with the left knee injected with saline as a control. One, eleven and twenty-one days after the injection of MIA solution, rats were anaesthetized with isoflurane inhalation, and 1 mg hydrocyanine (hydro-ICG) in 50μl saline was intra-articularly injected into both knees to image ROS production. Immediately following injections, rats were allowed to recover from anaesthesia and ambulate freely in their cages. A ten day interval between sequential injections was chosen to ensure clearance of the hydro-ICG probe from the joint and return of fluorescence intensity to the baseline level. One hour after injection of the hydro-ICG solution, rats were anaesthetized using isoflurane gas, and *in vivo* fluorescence images were captured via a Xenogen IVIS Lumina system (Caliper Life Sciences, Hopkinton, MA). The excitation and emission wavelengths for hydro-ICG were 745 and 840nm, and the exposure time was 12 seconds.

Assessment of Vascularity

Three-weeks after MIA injection, the rats that were used for ROS imaging were anaesthetized, maintained at the induction-level dose of isoflurane gas, and their vascular systems were sequentially perfused with 0.9% physiological saline solution, 10% neutral buffered formalin, and a lead chromate based contrast agent (Microfil MV-122, FlowTech, Carver, MA) via a needle passing through the left ventricle and into the aorta. This technique was slightly modified from a previously published methodology for contrast enhanced imaging of vascular structures (23). After polymerization overnight, both knee

joints were dissected to remove the attached muscles, and scanned by μCT at 45 kVp, 177 μA, 200 ms integration time, and a voxel size of 16 μm. Following demineralization with 10% formic acid for 10 days, both knee joints and dissected femora were scanned at 16 and 10 μm voxel size, respectively.

Statistical analysis

All data were expressed as mean ± standard deviation. Cartilage and bone morphology parameters and fluorescence intensities at different time points after MIA injection were evaluated using a one factor (time) repeated (left vs. right) general linear model with Tukey's test for post-hoc analysis. Vascularization between control and MIA injected knees was compared using paired t-tests. Statistical significance was set at $p = 0.05$ (SPSS 11, SPSS Inc., Chicago, IL).

Results

Representative images of femoral articular cartilage sections stained with safranin-O are shown in Fig. 1A. At one week post-injection, cartilage thickness and sGAG optical density in MIA cartilage decreased compared with control cartilage in the contralateral femora. At two and three weeks post-injection, part of the subchondral bone surface was denuded without cartilage coverage, especially in load-bearing regions of the condyles (Fig. 1A).

Representative images of 3-D morphology of rat femoral articular cartilage and bone are shown in Fig. 1B,C. Consistent with our previous studies (22, 24), we were able to segment cartilage from bone and therefore analyze cartilage in the 3-D EPIC-μCT images. At one week after injection, cartilage volume and normalized thickness (volume / bone surface interface area) from MIA-injected joints were 13% and 18% lower than contralateral control cartilage ($p<0.05$), respectively, while cartilage attenuation was 24% ($p<0.05$) higher than control cartilage. This suggested lower sulfated glycosaminoglycan (sGAG) content in MIA-treated femoral articular cartilage (22, 24) (Fig. 1B, Fig. 2). Trabecular bone volume fraction (BV/TV) and trabecular thickness (Tb.Th.) in the MIA-treated femoral epiphyses were 17% ($p<0.05$) and 10% ($p<0.01$) lower than controls, respectively (Fig. 1B, Fig. 3).

At two weeks post-injection, femoral articular cartilage volume, area and normalized thickness in MIA-injected joints were 26% ($p<0.05$), 19% ($p<0.01$), and 26% ($p<0.05$) lower than controls, respectively, and the attenuation was 24% ($p<0.01$) higher than controls (Fig. 2). An average of 12% of the surface was denuded subchondral bone with no cartilage coverage. BV/TV, connectivity density (Conn.D.), and Tb.Th. in the femoral epiphyses were 22%, 26%, and 7% ($p<0.01$ each) lower than controls, respectively (Fig. 3).

At three weeks after injection, femoral articular cartilage volume, area, and normalized thickness in MIA-injected joints were 12%, 22%, and 12% ($p<0.01$ each) lower than controls, respectively, while the attenuation was 16% higher than controls ($p<0.01$ Fig. 1C, Fig. 2). An average of 14% of the surface was denuded bone without cartilage coverage. BV/TV, Conn.D., and trabecular number (Tb.N.) in the femoral epiphysis were 20% ($p<0.01$), 20% ($p<0.05$), and 6% ($p<0.05$) lower than controls, respectively (Fig. 3).

In comparing within the control and MIA-injected joints, morphological but not compositional changes in femoral articular cartilage were seen over time. Femoral cartilage volume and normalized thickness were significantly lower in both of control and MIA-injected joints at two and three weeks compared to one week post-injection ($p<0.05$ or 0.01, Fig.2A,C). There was no significant difference in femoral cartilage attenuation among the three time points for either control or MIA-injected specimens (Fig.2D). With MIA injection, Conn.D. for trabecular bone in the femoral epiphysis was lower ($p<0.05$, Fig.3C)

while Tb.Th was higher ($P<0.05$, Fig.3E) at two and three weeks compared to one week after injection.

Representative fluorescence hydro-ICG ROS images (Fig. 4A) demonstrated that ROS quantities increased in MIA-induced OA knees, and this effect lessened with increased time after MIA injections. The fluorescence intensities in the right MIA-induced OA knee joints were 98% ($1.69\pm0.25 \times10^5$ vs. $0.86\pm0.51 \times10^5$ count/s, n=5, $p<0.05$, Fig. 4B) and 46% ($1.20\pm0.27 \times10^5$ vs. $0.82\pm0.09 \times10^5$ count/s, n=5, $p<0.05$) higher than those in the left contralateral control knee joints at 1 and 11 days after injections, respectively. However, the fluorescence intensity did not significantly differ ($0.54\pm0.12 \times10^5$ vs. $0.58\pm0.13 \times10^5$ count/s) between the control and OA knees at 21 days after injections. In comparing within the control and MIA-injected joints, the fluorescence intensity in the left saline control knee had no significant changes during the 21-day duration after injection. However, the fluorescence intensities in the right MIA-injected knee joints decreased by 29% (n=5, $p<0.05$) from 1- to 11-days after injection and further decreased by 54% from 11 to 21 days to reach the left control levels (n=5, $p<0.05$, Fig. 4B).

Three weeks after MIA-injection to induce OA, vascularization in both knee joints and distal femora was assessed (Fig. 5). Sagittal attenuation maps demonstrated erosions on the subchondral bone surfaces of the patella, femur and tibia in the OA knee joint (Fig. 5A). The main blood vessels perfused with contrast agent had higher attenuation (indicated in red) than the surrounding bone tissue indicated in yellow and green (Fig. 5A). The 3-D vascular network surrounding the knee joint, including all combined capsule, subchondral and trabecular bone, synovium, and meniscal tissues, is shown in Fig. 5B. The decalcified vascularity maps in Fig. 5C more clearly demonstrate the 3-D vascular distribution in the whole knee joint because mineral has been cleared and surrounding tissues are depicted transparently. Vessel volume, vessel volume fraction, and vessel connectivity density in the MIA-injected OA knee joints were 27% ($p<0.05$), 16% ($p<0.05$), and 44% ($p<0.01$) higher than those in the contralateral control joints, respectively (Fig. 5G–I). For the decalcified distal femur, sagittal sections of the attenuation maps are shown in Fig. 5D with red representing the larger main vessels. Segmented images of the vasculature with surrounding tissues depicted transparently are shown in Fig. 5E (lateral view) and Fig. 5F (distal view). Quantitative results showed similarity to results from the whole knee joint. Vessel volume, vessel volume fraction, and vessel connectivity density in the OA distal femora were 34% ($p<0.05$), 30% ($p<0.05$), and 60% ($p<0.05$) higher than those in the left femora (Fig. 5J–L).

Discussion

Current evaluation techniques for OA animal models, such as histological scoring and biochemical assays, are destructive, time consuming, and cannot assess the 3-D spatial morphology of articular cartilage and blood vessels. Cartilage histological scoring methods require scoring of approximately 10 sections across the whole knee joint, and the semi quantitative scores are subjective with intra-and inter-observer variation (25, 26). 3-D morphometric analyses obtained through μCT offer distinct advantages compared to 2-D histomorphometry: eliminating the need for exact specimen positioning and alignment (27), eliminating possible artifacts induced by sample fixation, dehydration, embedding and sectioning (28), providing more precise thickness measurements via sphere fitting and more complete quantitative volumetric assessments (29, 30). Following nondestructive μCT scanning with Hexabrix or Microfil contrast agents, most standard histologic processes, such as safranin-O staining in this study, can still be performed.

Microcomputed tomography (μCT) provides 3-D, quantitative morphologic analysis of hard tissues at micron-level voxel resolutions and has been used to monitor progressive changes

in the subchondral bone of rats injected with MIA (31). As the MIA-induced OA model is not a surgically-induced mechanical instability OA model, joints were not expected to show subchondral sclerosis or thickening of the subchondral bone plate, which has been observed in spontaneous OA guinea pigs (32), meniscectomy OA rabbits (33), anterior cruciate ligament transection (ACLT) rats (7), spontaneous OA mice (34), and OA patients (35, 36). Previous studies demonstrated thinner trabeculae in MIA- and collagenase-induced OA mouse models (37, 38). However, it was still surprising that only one week post-injection, significant decreases were observed in trabecular bone volume fraction and trabecular thickness in femoral epiphyses. The exact mechanism of the decrease in trabeculae is still unknown but potential causes may be skeletal disuse, inflammation, ROS, and the activation of osteoclasts (37). It has been shown that locomotor activity significantly decreases after MIA injection (20) due to the severe pain induced by inflammation in the MIA-injected OA knee joint (39). Accordingly, our results suggest that the change in trabecular volume fraction could provide a sensitive and quantitative index for disuse and pain.

Our previous studies indicated that EPIC-μCT imaging provides the ability to nondestructively assess cartilage morphology and composition in rat articular cartilage with high precision and accuracy (22, 24). In the present study, EPIC-μCT quantitatively depicted the temporal changes of 3-D cartilage morphology and composition in the rat distal femora in a MIA-induced OA model. Monosodium iodoacetate (MIA) inhibits the activity of glyceraldehyde-3-phosphate dehydrogenase in chondrocytes, resulting in disruption of glycolysis and eventually cell death (39). Destructive enzymatic activity causes proteoglycan degradation, chondrocyte necrobiosis and disruption of the collagen network, resulting in progressive impairment of mechanical function (40–43). This interaction between biochemical and mechanical factors created a progressive cycle for cartilage degradation and subchondral bone loss. The decrease of cartilage volume, area, thickness, and sGAG content were accompanied by the loss of trabecular bone and the erosion of subchondral bone surface in the distal femora, and these changes detected by μCT corresponded with results from histological evaluation. The ability to combine standard μCT and EPIC-μCT to quantitatively analyze cartilage and bone from the same joint provided improved understanding of the interactions between cartilage and bone during the progression of osteoarthritis.

Reactive oxygen species (ROS, superoxide and the hydroxyl radical) are toxic and could play an important role in the initiation and pathophysiology of OA (44). Current fluorescent probes, such as dihydroethidium, suffer from several problems that limit their wider application. Collaborators have developed a novel class of fluorescent sensors, hydrocyanines, that can image ROS *in vivo* (45, 46). Hydrocyanines have nanomolar sensitivity towards the hydroxyl radical with a linear response and are significantly more sensitive than the previous dihydroethidium probes. The fluorescence intensity in MIA-induced OA knees indicated that high levels of ROS were present in the synovial capsule one day after MIA injection and were gradually relieved by 21 days. This study demonstrated that *in vivo* fluorescence imaging can be used to noninvasively quantify ROS quantities during OA progression and pharmacological interventions in small animals. Additionally, the use of hydrocyanines to image ROS has the potential to be a powerful clinical tool to diagnose OA and monitor drug efficacy.

Recently, the perfusion of a radiodense contrast agent into blood vessels has allowed indirect nondestructive imaging of 3-D vascularity such that vascular volume, vessel thickness and connectivity density can be quantified post-mortem (47–50). This study demonstrated that μCT with contrast agent perfusion could be utilized to quantify 3-D vascularity in a small animal OA model, and for the first time indicated higher vascularity in OA whole knee joints and distal femora. These findings suggest the importance of

angiogenesis in the progression of OA, which is consistent with results showing that vascular invasion into subchondral bone contributes to cartilage degradation by expressing matrix metalloproteinases in OA (51). Although the exact mechanisms of angiogenesis in OA are still not clear, the high levels of ROS and early synovial inflammation indicated by joint swelling on day one post-injection is thought to play an important role in this pathological regeneration (16). ROS can induce VEGF expression (52), which may stimulate angiogenesis, and increased VEGF expression has been detected as early as 1 week post-surgery in the rat OA model, (12, 53). The combination of angiogenesis and ROS might also exacerbate the progression of cartilage degeneration and bone remodeling (17, 18, 54).

Providing a methodology that enables the creation of 3-D articular cartilage thickness and topography maps may impact many relevant applications. Using high-resolution 3-D cartilage thickness maps, focal variations in cartilage thickness can be visualized via the color scale, and the cartilage contact area and surface stresses can be estimated (29, 55). The thickness and topography maps can also be used to evaluate joint mechanics and mechano-adaptation of articular cartilage (56). In addition, these maps could be utilized to define the relationship between genetic background and cartilage phenotype (57) and to provide guidance in the design of prosthetic surfaces and tissue engineering constructs.

The MIA OA model is minimally invasive, reproducibly induces OA-like lesions, and has been widely used in OA animal studies (20, 31, 58, 59). One of the limitations of this study is the treatment of saline-injected contralateral limbs as controls rather than naïve, age-matched controls. The mobility of MIA mice decreased (20) while loading of the contralateral limbs increased compared to MIA-injected limbs, suggesting that the contralateral limb may not be truly normal. In this study, histology of the contralateral femora showed no apparent pathological changes in bone or cartilage, supporting the use of contralateral limbs as an internal control. Nevertheless, inclusion of age-matched control animals could provide additional insights into specific effects of MIA injection. MIA-induced arthritis is an aggressive model of cartilage degeneration and subchondral bone remodeling and is suitable for evaluating ROS, inflammation, pain and angiogenesis during OA progression. However, the aggressiveness of this model limits the ability of this study to elaborate on the relationship between cartilage degeneration and subchondral bone remodeling during early OA initiation. Further research is necessary to study multiple tissues via these novel techniques in more gradual settings such as spontaneous or surgically induced OA models, which are more similar to early human OA.

In summary, this is the first study to quantify the temporal changes in articular cartilage, subchondral bone, ROS, and vascularization in a rat MIA-induced OA model via fluorescence imaging and contrast-enhanced μCT. The ability to quantitatively evaluate changes in multiple tissues during the initiation and progression of OA may improve our understanding of the interactive changes in multiple tissues in OA pathophysiology and provide insights for new treatment modalities. This study established a drug evaluation platform to comprehensively evaluate potential disease modifying OA drugs. These advanced imaging techniques have the potential to become standardized analysis methods for comprehensive evaluation of articular joint degeneration and treatment efficacy.

Acknowledgments

This project was funded by NIH grant R21AR053716. The study sponsor had no involvement in the work described.

Sources of Support:

This project was funded by NIH grant R21AR053716.

References

1. Goldring MB, Goldring SR. Articular cartilage and subchondral bone in the pathogenesis of osteoarthritis. Ann N Y Acad Sci. 1192:230–237. [PubMed: 20392241]
2. Blair-Levy JM, Watts CE, Fiorentino NM, Dimitriadis EK, Marini JC, Lipsky PE. A type I collagen defect leads to rapidly progressive osteoarthritis in a mouse model. Arthritis Rheum. 2008; 58(4): 1096–1106. [PubMed: 18383364]
3. Mrosek EH, Lahm A, Erggelet C, Uhl M, Kurz H, Eissner B, et al. Subchondral bone trauma causes cartilage matrix degeneration: an immunohistochemical analysis in a canine model. Osteoarthritis Cartilage. 2006; 14(2):171–178. [PubMed: 16242359]
4. Radin EL, Rose RM. Role of subchondral bone in the initiation and progression of cartilage damage. Clin Orthop Relat Res. 1986; (213):34–40. [PubMed: 3780104]
5. Lajeunesse D, Reboul P. Subchondral bone in osteoarthritis: a biologic link with articular cartilage leading to abnormal remodeling. Curr Opin Rheumatol. 2003; 15(5):628–633. [PubMed: 12960492]
6. Antoniades L, MacGregor AJ, Matson M, Spector TD. A cotwin control study of the relationship between hip osteoarthritis and bone mineral density. Arthritis Rheum. 2000; 43(7):1450–1455. [PubMed: 10902745]
7. Hayami T, Pickarski M, Zhuo Y, Wesolowski GA, Rodan GA, Duong le T. Characterization of articular cartilage and subchondral bone changes in the rat anterior cruciate ligament transection and meniscectomized models of osteoarthritis. Bone. 2006; 38(2):234–243. [PubMed: 16185945]
8. Bettica P, Cline G, Hart DJ, Meyer J, Spector TD. Evidence for increased bone resorption in patients with progressive knee osteoarthritis: longitudinal results from the Chingford study. Arthritis Rheum. 2002; 46(12):3178–3184. [PubMed: 12483721]
9. Brandt KD, Dieppe P, Radin E. Etiopathogenesis of osteoarthritis. Med Clin North Am. 2009; 93(1):1–24. xv. [PubMed: 19059018]
10. Calvo E, Palacios I, Delgado E, Sanchez-Pernaute O, Largo R, Egido J, et al. Histopathological correlation of cartilage swelling detected by magnetic resonance imaging in early experimental osteoarthritis. Osteoarthritis Cartilage. 2004; 12(11):878–886. [PubMed: 15501403]
11. Ashraf S, Walsh DA. Angiogenesis in osteoarthritis. Curr Opin Rheumatol. 2008; 20(5):573–580. [PubMed: 18698180]
12. Bonnet CS, Walsh DA. Osteoarthritis, angiogenesis and inflammation. Rheumatology (Oxford). 2005; 44(1):7–16. [PubMed: 15292527]
13. Sutton S, Clutterbuck A, Harris P, Gent T, Freeman S, Foster N, et al. The contribution of the synovium, synovial derived inflammatory cytokines and neuropeptides to the pathogenesis of osteoarthritis. Vet J. 2009; 179(1):10–24. [PubMed: 17911037]
14. Case JP, Baliunas AJ, Block JA. Lack of efficacy of acetaminophen in treating symptomatic knee osteoarthritis: a randomized, double-blind, placebo-controlled comparison trial with diclofenac sodium. Arch Intern Med. 2003; 163(2):169–178. [PubMed: 12546607]
15. Hellio Le Graverand-Gastineau MP. OA clinical trials: current targets and trials for OA Choosing molecular targets: what have we learned and where we are headed? Osteoarthritis Cartilage. 2009
16. Costa C, Incio J, Soares R. Angiogenesis and chronic inflammation: cause or consequence? Angiogenesis. 2007; 10(3):149–166. [PubMed: 17457680]
17. Imhof H, Breitenseher M, Kainberger F, Trattnig S. Degenerative joint disease: cartilage or vascular disease? Skeletal Radiol. 1997; 26(7):398–403. [PubMed: 9259096]
18. Haywood L, McWilliams DF, Pearson CI, Gill SE, Ganesan A, Wilson D, et al. Inflammation and angiogenesis in osteoarthritis. Arthritis Rheum. 2003; 48(8):2173–2177. [PubMed: 12905470]
19. Mapp PI, Avery PS, McWilliams DF, Bowyer J, Day C, Moores S, et al. Angiogenesis in two animal models of osteoarthritis. Osteoarthritis Cartilage. 2008; 16(1):61–69. [PubMed: 17659886]
20. Guingamp C, Gegout-Pottie P, Philippe L, Terlain B, Netter P, Gillet P. Monoiodoacetate- induced experimental osteoarthritis: a dose-response study of loss of mobility, morphology, and biochemistry. Arthritis Rheum. 1997; 40(9):1670–1679. [PubMed: 9324022]

21. Palmer AW, Guldberg RE, Levenston ME. Analysis of cartilage matrix fixed charge density and three-dimensional morphology via contrast-enhanced microcomputed tomography. Proc Natl Acad Sci U S A. 2006; 103(51):19255–19260. [PubMed: 17158799]
22. Xie L, Lin AS, Levenston ME, Guldberg RE. Quantitative assessment of articular cartilage morphology via EPIC-microCT. Osteoarthritis Cartilage. 2009; 17(3):313–320. [PubMed: 18789727]
23. Duvall CL, Taylor WR, Weiss D, Guldberg RE. Quantitative microcomputed tomography analysis of collateral vessel development after ischemic injury. Am J Physiol Heart Circ Physiol. 2004; 287(1):H302–H310. [PubMed: 15016633]
24. Xie L, Lin AS, Guldberg RE, Levenston ME. Nondestructive assessment of sGAG content and distribution in normal and degraded rat articular cartilage via EPIC-microCT. Osteoarthritis Cartilage. 18(1):65–72. [PubMed: 19744590]
25. Gerwin N, Bendele AM, Glasson S, Carlson CS. The OARSI histopathology initiative - recommendations for histological assessments of osteoarthritis in the rat. Osteoarthritis Cartilage. 18(Suppl 3):S24–S34. [PubMed: 20864021]
26. Glasson SS, Chambers MG, Van Den Berg WB, Little CB. The OARSI histopathology initiative - recommendations for histological assessments of osteoarthritis in the mouse. Osteoarthritis Cartilage. 18(Suppl 3):S17–S23. [PubMed: 20864019]
27. Xia Y. The total volume and the complete thickness of articular cartilage determined by MRI. Osteoarthritis Cartilage. 2003; 11(7):473–474. [PubMed: 12814609]
28. Uchiyama T, Tanizawa T, Muramatsu H, Endo N, Takahashi HE, Hara T. A morphometric comparison of trabecular structure of human ilium between microcomputed tomography and conventional histomorphometry. Calcif Tissue Int. 1997; 61(6):493–498. [PubMed: 9383277]
29. Millington SA, Grabner M, Wozelka R, Anderson DD, Hurwitz SR, Crandall JR. Quantification of ankle articular cartilage topography and thickness using a high resolution stereophotography system. Osteoarthritis Cartilage. 2007; 15(2):205–211. [PubMed: 16949841]
30. Laib A, Barou O, Vico L, Lafage-Proust MH, Alexandre C, Rugsegger P. 3D micro-computed tomography of trabecular and cortical bone architecture with application to a rat model of immobilisation osteoporosis. Med Biol Eng Comput. 2000; 38(3):326–332. [PubMed: 10912350]
31. Morenko BJ, Bove SE, Chen L, Guzman RE, Juneau P, Bocan TM, et al. In vivo micro computed tomography of subchondral bone in the rat after intra-articular administration of monosodium iodoacetate. Contemp Top Lab Anim Sci. 2004; 43(1):39–43. [PubMed: 14984289]
32. Anderson-MacKenzie JM, Quasnichka HL, Starr RL, Lewis EJ, Billingham ME, Bailey AJ. Fundamental subchondral bone changes in spontaneous knee osteoarthritis. Int J Biochem Cell Biol. 2005; 37(1):224–236. [PubMed: 15381164]
33. Fahlgren A, Messner K, Aspenberg P. Meniscectomy leads to an early increase in subchondral bone plate thickness in the rabbit knee. Acta Orthop Scand. 2003; 74(4):437–441. [PubMed: 14521295]
34. Wachsmuth L, Engelke K. High-resolution imaging of osteoarthritis using microcomputed tomography. Methods Mol Med. 2004; 101:231–248. [PubMed: 15299218]
35. Ding M, Odgaard A, Hvid I. Changes in the three-dimensional microstructure of human tibial cancellous bone in early osteoarthritis. J Bone Joint Surg Br. 2003; 85(6):906–912. [PubMed: 12931817]
36. Hochberg MC, Lethbridge-Cejku M, Tobin JD. Bone mineral density and osteoarthritis: data from the Baltimore Longitudinal Study of Aging. Osteoarthritis Cartilage. 2004; 12(Suppl A):S45–S48. [PubMed: 14698641]
37. Botter SM, van Osch GJ, Waarsing JH, van der Linden JC, Verhaar JA, Pols HA, et al. Cartilage damage pattern in relation to subchondral plate thickness in a collagenase-induced model of osteoarthritis. Osteoarthritis Cartilage. 2008; 16(4):506–514. [PubMed: 17900935]
38. Koh YH, Hong SH, Kang HS, Chung CY, Koo KH, Chung HW, et al. The effects of bone turnover rate on subchondral trabecular bone structure and cartilage damage in the osteoarthritis rat model. Rheumatol Int. 30(9):1165–1171. [PubMed: 19711077]

39. Beyreuther B, Callizot N, Stohr T. Antinociceptive efficacy of lacosamide in the monosodium iodoacetate rat model for osteoarthritis pain. Arthritis Res Ther. 2007; 9(1):R14. [PubMed: 17284318]
40. Armstrong CG, Mow VC. Variations in the intrinsic mechanical properties of human articular cartilage with age, degeneration, and water content. J Bone Joint Surg Am. 1982; 64(1):88–94. [PubMed: 7054208]
41. Williamson AK, Chen AC, Sah RL. Compressive properties and function-composition relationships of developing bovine articular cartilage. J Orthop Res. 2001; 19(6):1113–1121. [PubMed: 11781013]
42. Rieppo J, Toyras J, Nieminen MT, Kovanen V, Hyttinen MM, Korhonen RK, et al. Structure-function relationships in enzymatically modified articular cartilage. Cells Tissues Organs. 2003; 175(3):121–132. [PubMed: 14663155]
43. LeRoux MA, Arokoski J, Vail TP, Guilak F, Hyttinen MM, Kiviranta I, et al. Simultaneous changes in the mechanical properties, quantitative collagen organization, and proteoglycan concentration of articular cartilage following canine meniscectomy. J Orthop Res. 2000; 18(3): 383–392. [PubMed: 10937624]
44. Regan E, Flannelly J, Bowler R, Tran K, Nicks M, Carbone BD, et al. Extracellular superoxide dismutase and oxidant damage in osteoarthritis. Arthritis Rheum. 2005; 52(11):3479–3491. [PubMed: 16255039]
45. Kundu K, Knight SF, Willett N, Lee S, Taylor WR, Murthy N. Hydrocyanines: a class of fluorescent sensors that can image reactive oxygen species in cell culture, tissue, and in vivo. Angew Chem Int Ed Engl. 2009; 48(2):299–303. [PubMed: 19065548]
46. Lee D, Khaja S, Velasquez-Castano JC, Dasari M, Sun C, Petros J, et al. In vivo imaging of hydrogen peroxide with chemiluminescent nanoparticles. Nat Mater. 2007; 6(10):765–769. [PubMed: 17704780]
47. Garcia-Sanz A, Rodriguez-Barbero A, Bentley MD, Ritman EL, Romero JC. Three-dimensional microcomputed tomography of renal vasculature in rats. Hypertension. 1998; 31(1 Pt 2):440–444. [PubMed: 9453342]
48. Jorgensen SM, Demirkaya O, Ritman EL. Three-dimensional imaging of vasculature and parenchyma in intact rodent organs with X-ray micro-CT. Am J Physiol. 1998; 275(3 Pt 2):H1103–H1114. [PubMed: 9724319]
49. Paulus MJ, Gleason SS, Kennel SJ, Hunsicker PR, Johnson DK. High resolution X-ray computed tomography: an emerging tool for small animal cancer research. Neoplasia. 2000; 2(1–2):62–70. [PubMed: 10933069]
50. Bentley MD, Ortiz MC, Ritman EL, Romero JC. The use of microcomputed tomography to study microvasculature in small rodents. Am J Physiol Regul Integr Comp Physiol. 2002; 282(5):R1267–R1279. [PubMed: 11959666]
51. Shibakawa A, Yudoh K, Masuko-Hongo K, Kato T, Nishioka K, Nakamura H. The role of subchondral bone resorption pits in osteoarthritis: MMP production by cells derived from bone marrow. Osteoarthritis Cartilage. 2005; 13(8):679–687. [PubMed: 15961327]
52. Fay J, Varoga D, Wruck CJ, Kurz B, Goldring MB, Pufe T. Reactive oxygen species induce expression of vascular endothelial growth factor in chondrocytes and human articular cartilage explants. Arthritis Res Ther. 2006; 8(6):R189. [PubMed: 17187682]
53. Hayami T, Funaki H, Yaoeda K, Mitui K, Yamagiwa H, Tokunaga K, et al. Expression of the cartilage derived anti-angiogenic factor chondromodulin-I decreases in the early stage of experimental osteoarthritis. J Rheumatol. 2003; 30(10):2207–2217. [PubMed: 14528519]
54. Henrotin Y, Kurz B, Aigner T. Oxygen and reactive oxygen species in cartilage degradation: friends or foes? Osteoarthritis Cartilage. 2005; 13(8):643–654. [PubMed: 15936958]
55. Koo S, Gold GE, Andriacchi TP. Considerations in measuring cartilage thickness using MRI: factors influencing reproducibility and accuracy. Osteoarthritis Cartilage. 2005; 13(9):782–789. [PubMed: 15961328]
56. Eckstein F, Reiser M, Englmeier KH, Putz R. In vivo morphometry and functional analysis of human articular cartilage with quantitative magnetic resonance imaging--from image to data, from data to theory. Anat Embryol (Berl). 2001; 203(3):147–173. [PubMed: 11303902]

57. Botter SM, van Osch GJ, Waarsing JH, van der Linden JC, Verhaar JA, Pols HA, et al. Cartilage damage pattern in relation to subchondral plate thickness in a collagenase-induced model of osteoarthritis. Osteoarthritis Cartilage. 2007

58. Guzman RE, Evans MG, Bove S, Morenko B, Kilgore K. Mono-iodoacetate-induced histologic changes in subchondral bone and articular cartilage of rat femorotibial joints: an animal model of osteoarthritis. Toxicol Pathol. 2003; 31(6):619–624. [PubMed: 14585729]

59. Piscaer TM, Waarsing JH, Kops N, Pavljasevic P, Verhaar JA, van Osch GJ, et al. In vivo imaging of cartilage degeneration using microCT-arthrography. Osteoarthritis Cartilage. 2008; 16(9):1011–1017. [PubMed: 18342549]

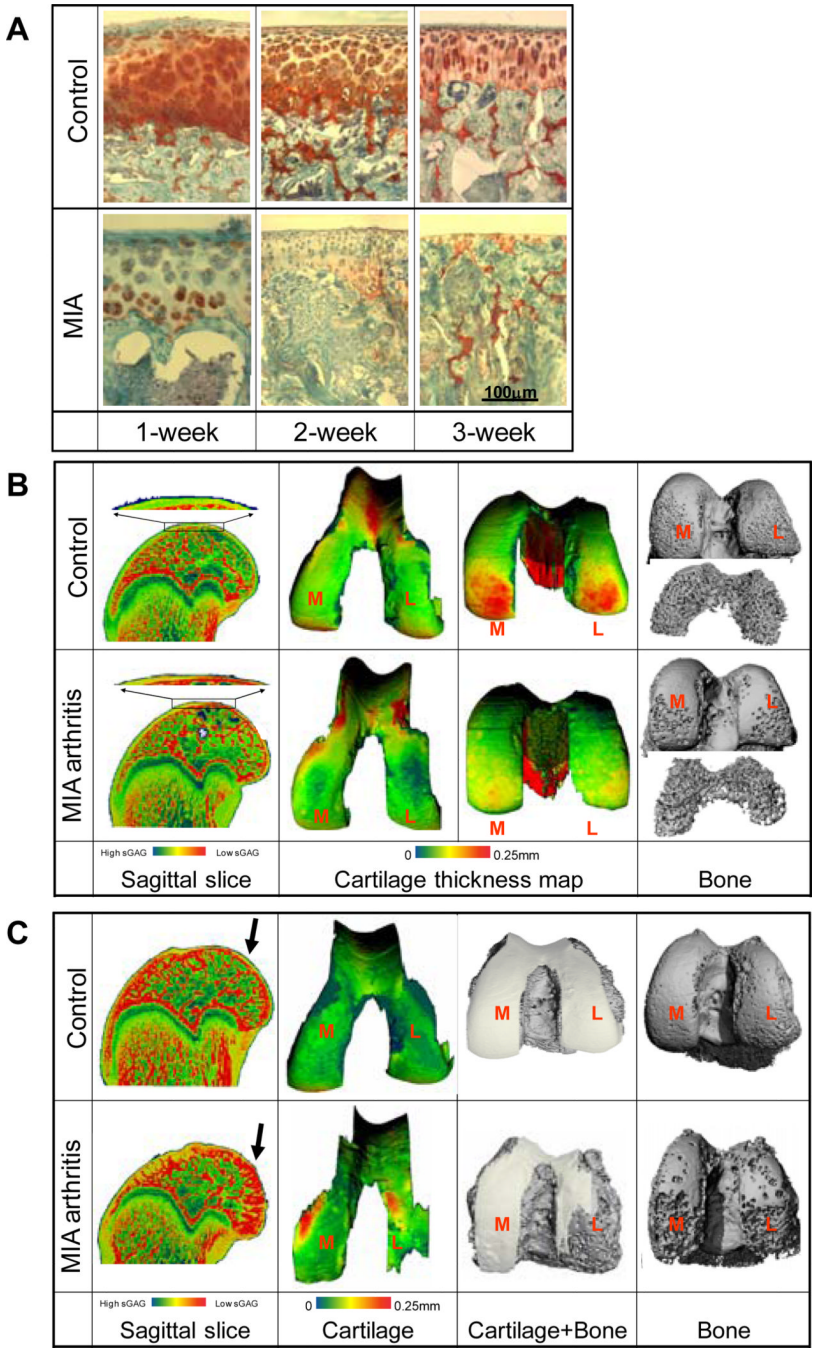

Figure 1.

A: Representative safranin-O stained sagittal sections of femoral articular cartilage in saline control and MIA-injected knees at 1, 2, and 3 weeks post-injection. **B-C**: EPIC-μCT images of cartilage X-ray attenuation (sagittal slices), cartilage thickness maps, and standard μCT images of subchondral and trabecular bone in distal femora at 1 week (**B**) and 3 weeks (**C**) after injections of MIA to induce OA and saline for contralateral controls.

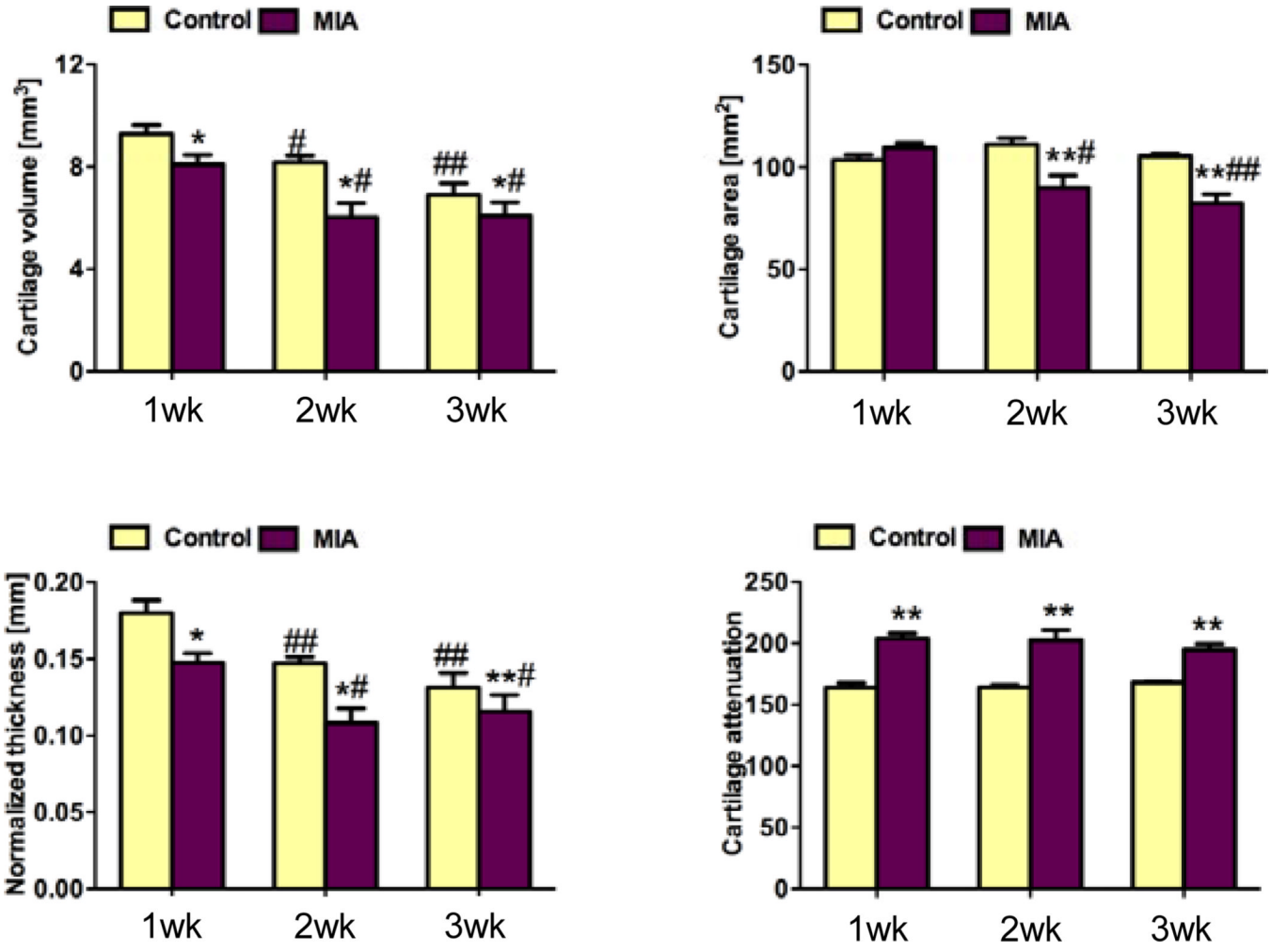

Figure 2.

Cartilage properties quantified in the distal femoral condyles for control and MIA-injected knees after 1, 2, and 3 weeks. **A**: cartilage volume; **B**: cartilage area; **C**: cartilage normalized thickness; **D**: cartilage attenuation. At 1 week post-injection, cartilage volume and normalized thickness (volume / bone surface interface area) from MIA-injected joints were significantly lower than contralateral control cartilage. At 2 and 3 weeks post-injection, cartilage volume, area and normalized thickness of MIA-injected cartilage were significantly lower than controls. Average cartilage attenuation was significantly higher than controls at all time points. * $p<0.05$ vs. left control, ** $p<0.01$ vs. left control, # $p<0.05$ vs. 1 week post-injection, ## $p<0.01$ vs. 1 week post-injection.

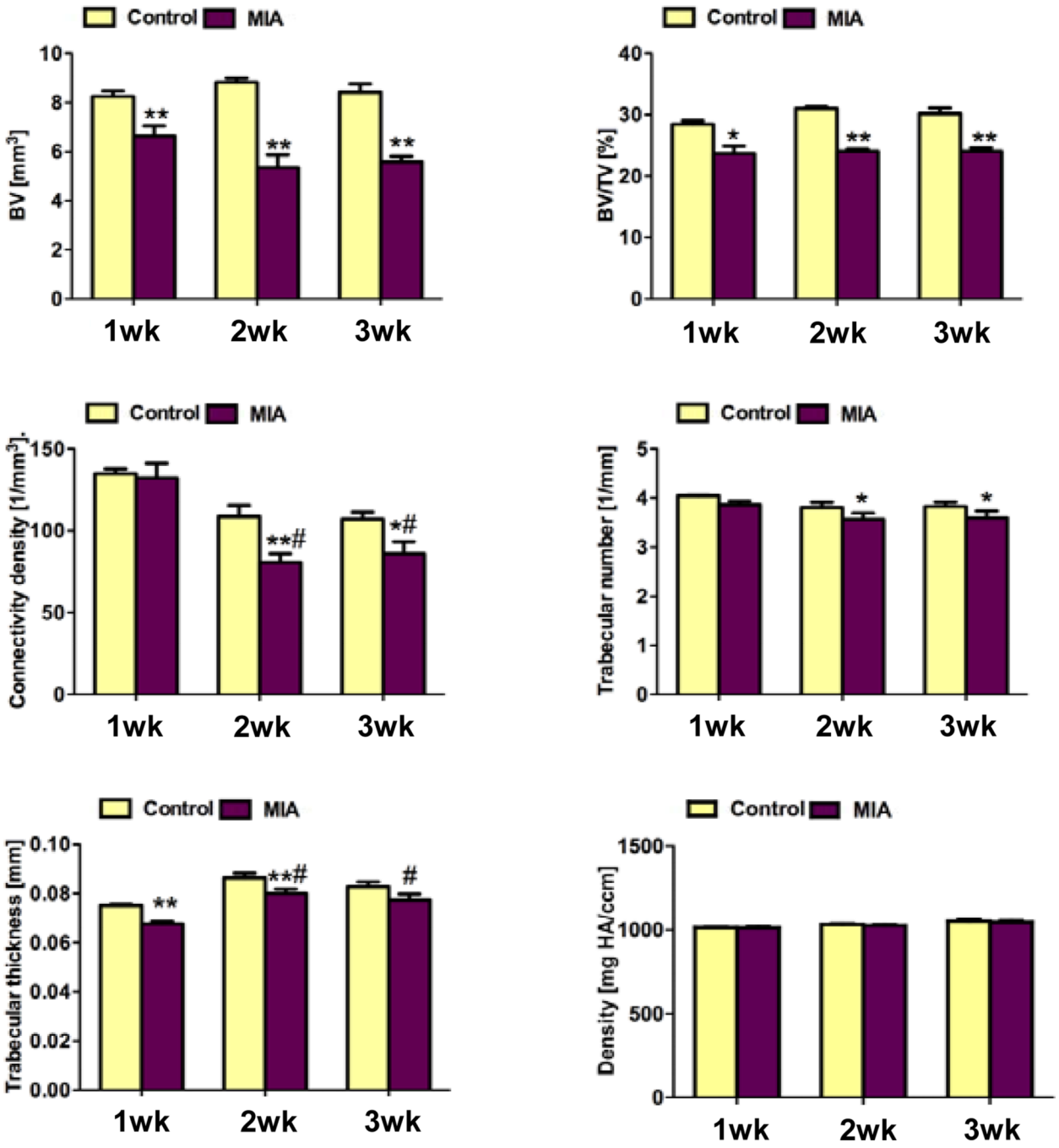

Figure 3.

Trabecular bone morphometry quantified in the distal femoral epiphyses of control and MIA-injected knee joints after 1, 2, and 3 weeks. A: trabecular bone volume (BV); B: trabecular bone volume fraction (BV/TV); C: connectivity density (Conn.D.); D: trabecular number (Tb.N.); E: trabecular thickness (Tb.Th.); F: Bone mineral density. At 1 week post-injection, BV/TV and Tb.Th. in the MIA-treated femoral epiphyses were significantly lower than in the contralateral epiphyses. At 2 weeks post-injection, BV/TV, Conn.D., and Tb.Th. for the MIA-injected knees were significantly lower than controls. At 3 weeks post-injection, BV/TV, Conn.D., and Tb.N. in the femoral epiphyses were significantly lower than controls. Average bone mineral densities in MIA-treated femora were not significantly

different from controls at any of the three time points. * $p<0.05$ vs. left control, ** $p<0.01$ vs. left control, # $p<0.05$ vs. 1 week post-injection.

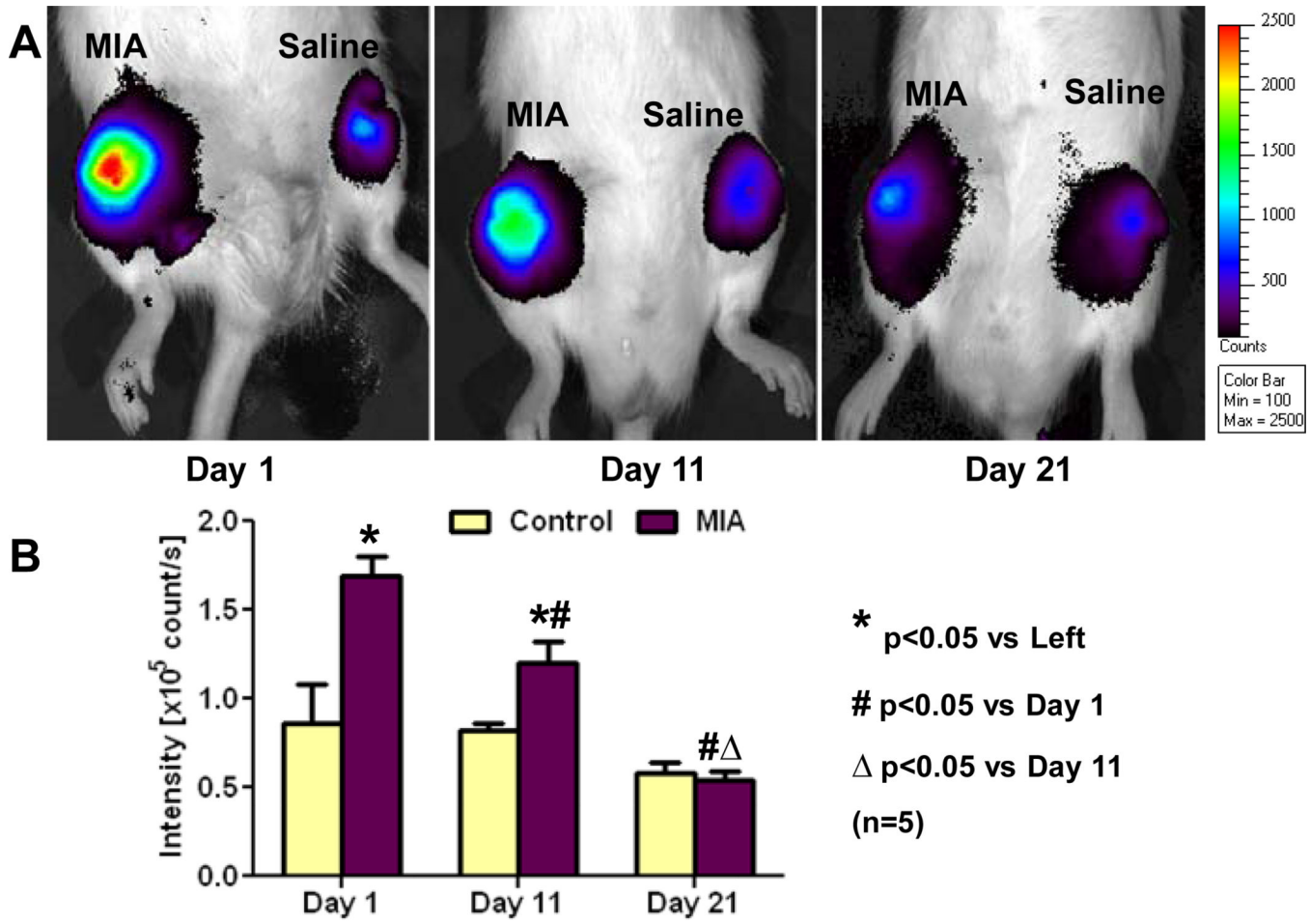

Figure 4.

Fluorescence imaging of reactive oxygen species (ROS) as an indicator of inflammatory response in MIA-induced OA rat joints and their contralateral controls. **A**: Representative hydro-ICG ROS images at 1, 11, and 21 days post-injection. **B**: MIA-injected knees showed a significant difference in fluorescence intensity at 1 and 11 days post-injection, but this difference was not seen at 21 days. For MIA-injected joints, significant time dependent decreases in fluorescence intensity were seen, but the control joints showed no significant differences over time. * $p<0.05$ vs. left control, # $p<0.05$ vs. 1 day post-injection, Δ $p<0.05$ vs. 11 days post-injection.

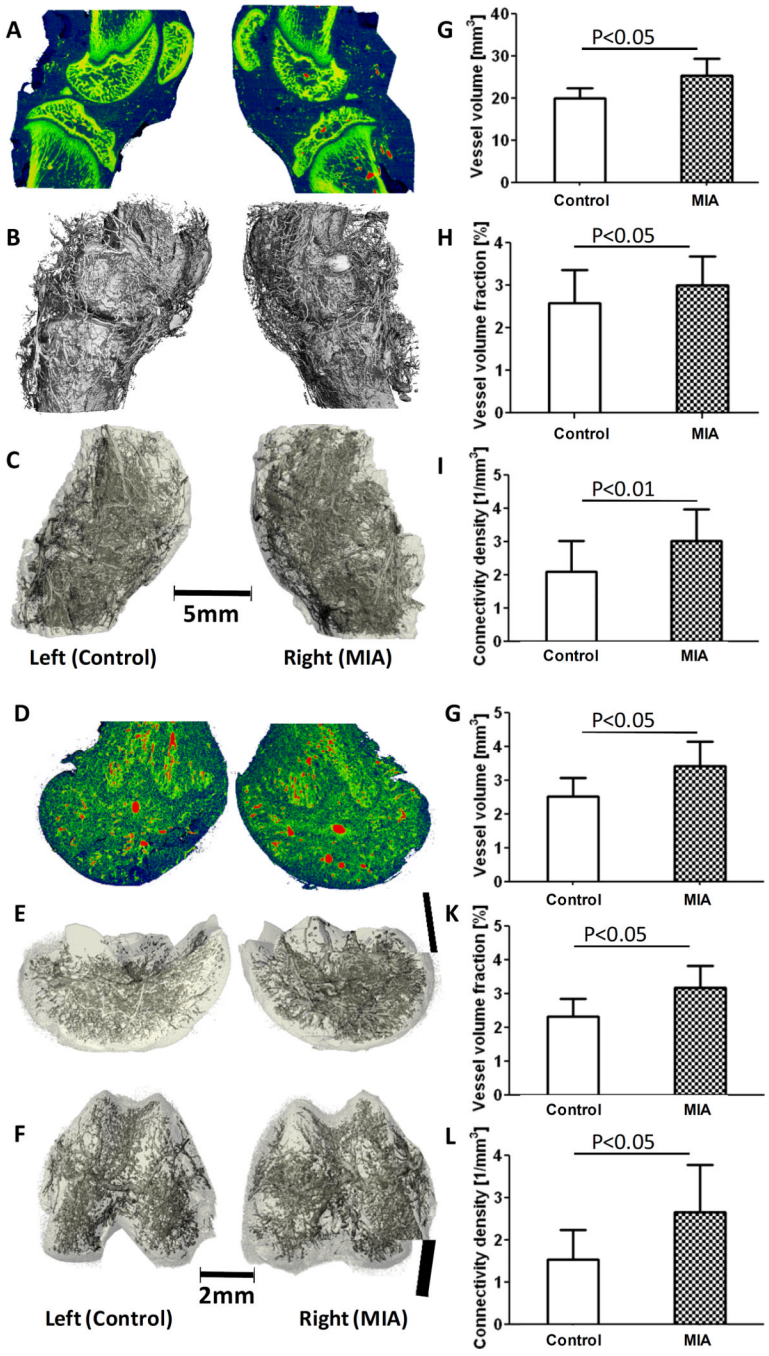

Figure 5.

Assessment of vascularization three weeks after MIA-injection to induce OA in rat knee joints. **A**: Representative sagittal section X-ray attenuation maps for MIA-induced and control joints, including bone and vasculature. Red represents the higher attenuating contrast-perfused vasculature, and green/yellow represents bone. **B**: Segmented μCT image including both bone and vasculature in the whole joints. **C**: Post-decalcification image depicting the full 3-D vascular network within and surrounding the joints. **D**: Sagittal section of X-ray attenuation maps for the decalcified distal femora. Red indicates higher attenuating main vasculature, and green indicates the smaller surrounding vessels. **E**: Segmented 3-D

μCT image of vasculature within the distal femora (lateral view). **F**: Segmented 3-D μCT image of distal femora (distal condylar view). **G-I**: Results showed a significant increase in vascular volume (**G**), vascular volume fraction (**H**), and connectivity density (**I**) with MIA-injected joints vs. contralateral controls after 3 weeks. **J-L**: In the isolated distal femora, similarly to whole joint results, increases in vascular volume (**J**), vascular volume fraction (**K**), and connectivity density (**L**) were seen.